Available online at www.sciencedirect.com
SCIENCE DIRECT®
Journal of Membrane Science 274 (2006) 92–101
journal of MEMBRANE SCIENCE
www.elsevier.com/locate/memsci

Different oxides used as diffusion barriers in composite hydrogen permeable membranes

D. Yepes, L.M. Cornaglia*, S. Irusta, E.A. Lombardo

Instituto de Investigaciones en Catálisis y Petroquímica (FIQ, UNL-CONICET), Santiago del Estero 2829-3000, Santa Fe, Argentina

Received 14 June 2005; received in revised form 4 August 2005; accepted 9 August 2005
Available online 23 September 2005

Abstract

Composite Pd–Ag membranes supported on modified porous stainless steel substrates were prepared by sequential electroless plating. To improve the stability of the Pd–Ag alloy, two different intermediate layers of α-Fe_2O_3 and γ-Al_2O_3 oxides were employed as diffusion barriers. A new activation method was also investigated which consisted in the impregnation of a layer of Pd supported γ-Al_2O_3 to generate palladium seeds. The membranes were studied by XRD, Auger depth profiling, SEM and EPMA. They were tested in a gas permeation system to determine the hydrogen permeability and selectivity. The Pd–Ag/PSS membranes had a good thermal resistance. The membranes prepared with alumina diffusion barriers exhibited lower ideal selectivity than the Pd–Ag/α-Fe_2O_3/PSS. However, the former membranes had two times higher hydrogen permeability. The Auger depth profiles did not show the presence of Fe in the Pd–Ag film, indicating that the γ-Al_2O_3 layer effectively blocked the intermetallic diffusion.

Keywords: Pd–Ag membrane; Diffusion barrier; Alumina layer

1. Introduction

The demand for hydrogen has increased in recent years since it is essential for the production of clean fuel. Palladium-based membranes are very important for hydrogen production because of their potential use in hydrogen purification or in membrane reactors [1–4]. The hydrogen embrittlement of pure palladium membranes [5] can be overcome by alloying palladium with silver. In this way, the α–β Pd–H transition temperature significantly decreases thus improving the membrane thermal stability. In addition, the presence of silver also enhances hydrogen permeation flux with no detrimental effects on its selectivity [6]. The optimum silver concentration is in the region of 23 wt.% silver [7].

The structure of the support employed has a significant effect on the permeance of the composite membranes. Nam et al. [8] found that the top layer features of the substrate strongly affected the quality of the Ag/Pd deposit. Roughness, large pore size, and defects present in the substrate before deposition are largely responsible for the membrane not being completely pinhole-free. The thermal expansion coefficient of stainless steel is close to that of palladium. However, the atomic inter-diffusion of metals between the palladium-based film and the substrate materials occurring at high temperature can deteriorate the performance of the palladium alloy membrane. The application of a diffusion barrier could inhibit the interface reactions between the neighboring layers. Nam and Lee [5] introduced an intermediate layer of silica as a diffusion barrier between the palladium alloy layer and the stainless steel substrate. They observed that the barrier modified the surface properties of the substrate, such as pore size and roughness. Micro-structural rearrangements took place, which resulted in a decrease in the size or number of pinholes and/or a decrease of the inter-crystalline spacing that forms diffusion pathways for nitrogen gas. The improved membranes were structurally stable and much more efficient for hydrogen permeances than those without diffusion barriers. Wang et al. [9] in a palladium membrane supported on porous stainless steel modified with zirconium oxide particles, found that the hydrogen flux was lower than that of a palladium membrane prepared on a porous glass. The internal pores of zirconium oxide particles offer resistance to hydrogen diffusion.

* Corresponding author. Tel.: +54 342 4536861; fax: +54 342 4571162.
E-mail address: nfisico@fiqus.unl.edu.ar (L.M. Cornaglia).

0376-7388/$ – see front matter © 2005 Elsevier B.V. All rights reserved.
doi:10.1016/j.memsci.2005.08.003

Mardilovich and coworkers [10] developed a controlled in situ oxidation of the porous stainless steel prior to plating in order to produce an oxide layer acting as a diffusion barrier between Pd and PSS. They claimed that Cr_2O_3 is the most desirable oxide phase due to its high chemical stability under hydrogen atmosphere. However, a thick oxide layer was formed on the support oxidized at 800 °C. It was made of an iron-rich layer sitting on top of a mixed Cr and Fe oxide phase.

Among the methods developed to deposit Pd or Pd-alloy films, electroless plating gives uniform deposition on complex shapes, produces hardness on the deposited film, and requires very simple equipment [11]. Electroless plating has been used to produce Pd and Pd alloy membranes on porous glass, alumina [11] and porous stainless steel [12]. Prior to the electroless plating of palladium and silver, the surface of substrates must be activated by seeding the metal nuclei [6]. Conventional seeding involves immersions in acid tin and palladium solutions. Previously, Li et al. [13] developed a preparation technique to pre-seed palladium nuclei on ceramic substrates, by which the sensitization and activation processes could be omitted. A γ-Al_2O_3 layer was deposited on the surface of the alumina support by the sol–gel technique employing a sol modified with a palladium chloride solution. The authors found that the Pd nuclei tightly adsorbed on the γ-Al_2O_3 top layer were evenly distributed, well dispersed and exhibited high catalytic activity. Consequently, the rate of palladium deposition was greater over the Pd modified γ-Al_2O_3 top layer.

In the present work, we investigated the improvement of the structural stability of the Pd–Ag composite membranes by introducing three different diffusion barriers, i.e. thin layers of either α-Fe_2O_3, γ-Al_2O_3 or Pd activated γ-alumina. The membranes were characterized by XRD, SEM, Auger electron spectroscopy (AES) and permeation measurements.

2. Experimental

2.1. Membrane synthesis

Employing the electroless plating method, palladium and silver were deposited on the outer surface of the porous stainless steel (PSS) support tube provided by Mott Metallurgical [11]. The stainless steel tube was 40 mm in length with an outside diameter of 10 mm and a wall thickness of 1.6 mm. The average pore size was 0.2 μm. Prior to deposition, the PSS was welded to a non-porous stainless steel tube and then the support was sonicated with acetone to remove organic contaminants and dirt. Afterwards, the support was modified employing different procedures: (i) The cleaned support was oxidized with air at 800 °C for 12 h. The rate of heating and cooling during the oxidation treatment was 1 °C/min. (ii) The washcoat with γ-Al_2O_3 was performed using a suspension made up of 15 wt.% of γ-Al_2O_3 (BUEHLER, 0.05 μm) in acid deionized water (pH 4.5). Three successive dippings of the support were performed and after each immersion, air was blown to eliminate the excess. Afterwards, the substrate was calcined in air at 500 °C for 6 h. (iii) The washcoat of (Pd)γ-Al_2O_3 was performed employing a 15 wt.% γ-Al_2O_3 suspension in acidic $PdCl_2$ solution (pH 4.5). Then, the substrate was dried at 110 °C and calcined at 500 °C followed by a reduction in hydrogen flow during 2 h.

Table 1
Composition of plating solutions and electroless plating conditions

Precursors and conditions	Pd solution concentration	Ag solution concentration
$PdCl_2$ (g/L)	3.6	–
$AgNO_3$ (g/L)	–	4.9
HCl (37 wt.%) (mL/L)	5.0	–
Na_2EDTA (g/L)	67	33.6
NH_4OH (28 wt.%) (mL/L)	650	650
N_2H_4 (1 M) (mL/L)	10	5
Temperature (°C)	50–55	45
pH	∼11.0	∼11.0

The modified substrates [(i) and (ii)] were activated by the conventional Pd–Sn activation procedure [6]. The PSS membranes were plated using a sequential deposition of Pd and Ag by electroless plating. First, two depositions of Pd were applied, followed by one deposition of silver and then another Pd layer was plated. This complete process was repeated twice to obtain a sufficiently high coverage of the Pd–Ag film. The compositions of the electroless plating baths are shown in Table 1. After deposition, the as-deposited membrane was rinsed with deionized water and then dried in an oven for 10 h at 100 °C. The membranes were heated in a helium flow at 650 °C during 72 or 120 h. Before the first measurement of hydrogen permeability, the membranes were activated in a hydrogen flow for 8 h at 400 °C.

2.2. SEM and EPMA characterization

The morphology and microstructure of the Pd–Ag film was imaged using a scanning electron microscope JEOL, model JSM-35 C, equipped with an energy dispersive analytical system (EDAX) for microprobe analysis.

2.3. Auger depth profile

Measurements were performed in a commercial ultra high vacuum (UHV) surface analysis system with a base pressure in the 10^{-10} Torr range. Differentiated Auger spectra were acquired using a single-pass cylindrical mirror analyzer (CMA) with a resolution of 0.6% and 2 V_{p-p} modulation amplitude. The experiment was accomplished by sputtering the sample surface using a 5 keV Ar^+ beam. The Auger peak areas of the kinetic energy transitions 318.0–341, 342–366.0, 680–731 and 550–500 eV were integrated and normalized to represent the relative quantities of Pd, Ag, Fe and O, respectively. A linear relationship between the Auger electron intensity and the concentration was assumed.

2.4. Optical microscopy

The membranes were observed using a NIKON OPTIPHOT zoom microscope connected to an FX-35DX NIKON camera.

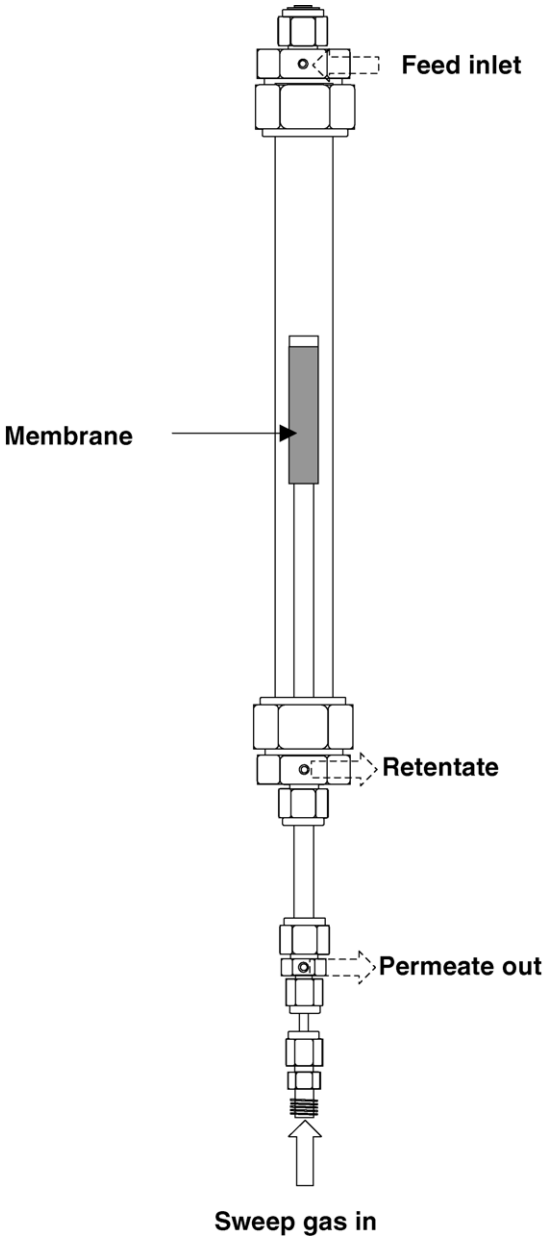

Fig. 1. Membrane module scheme.

2.5. X-ray diffraction

The XRD patterns of the films were obtained with an XD-D1 Shimadzu instrument, using Cu Kα radiation at 30 kV and 40 mA. The scan rate was 1°/min in the range $2\theta = 10–80°$.

2.6. Gas permeation measurements

Thermal treatments and gas permeation measurements were conducted in a shell-and-tube membrane module shown in Fig. 1. The open end of the membrane was sealed to the permeator wall with Teflon ferrules. The permeator was placed in an electrical furnace and heated to the desired temperatures. A thermocouple within the membrane tube monitored and controlled the temperature during the experiments. Various gases were used as permeation gases, including pure hydrogen, nitrogen and argon and mixed feeds of H_2 and N_2. All gases were fed to the permeator using calibrated mass-flow controllers. Feed gases flowed along the outside of the membrane and the permeated gases were measured in the inner side of the membrane. An Ar sweep gas stream was introduced in the permeated side only during the annealing process. A six-way valve connected with a sample loop allowed for injection of either the permeate or the retentate stream in the gas chromatograph unit SRI 8610C. The composition analysis was performed with the aid of a molecular sieve column and a TCD detector. Pressure differences across the membranes were obtained using a back-pressure regulator to vary the pressure on the upstream side and keeping the pressure constant downstream at 1 bar. The gas permeation rates were measured using two bubble flow meters at room temperature and pressure.

3. Results and discussion

3.1. Diffusion barrier formation

Three different diffusion barriers were used to condition the surface properties of the porous stainless steel tube. These barriers were applied to block the intermetallic diffusion of the PSS components to the Pd–Ag film.

3.1.1. Oxides as diffusion barriers

The first barrier investigated was the formation of several oxides by oxidation of the elements that make up the PSS support. The oxidation process was followed by XRD, SEM, Auger electron depth profiling and optical microscopy.

Fig. 2a shows the X-ray diffraction pattern of the PSS substrate. The reflection peaks at $2\theta = 43.6°$, 50.8° and 74.7° are assigned to the γ-Fe (fcc) structure; the reflection peak at 44.7° could correspond to the α-Fe phase. The substrate oxidation process at 800 °C leads to the formation of metal oxides. The XRD

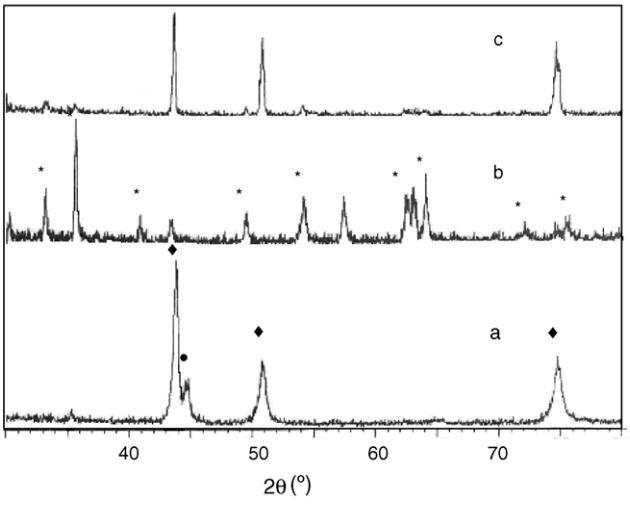

Fig. 2. X-ray diffraction patterns of the porous stainless steel substrates: (a) original substrate, (b) after oxidation in air at 800 °C for 12 h and (c) after washcoating with γ-Al_2O_3. Symbols: (●) α-Fe, (♦) γ-Fe and (*) α-Fe_2O_3.

pattern after this treatment is shown in Fig. 2b. The α-Fe_2O_3 phase is identified by comparison with the diffraction pattern reported by Marchetti et al. [14]. Other minor reflection peaks are observed, even though they are difficult to be assigned. They could be related to oxides of the other elements of the stainless steel (Ni, Cr, etc.).

To check the existence of a Cr-rich oxide layer, Mardilovich and coworkers [10] performed an EDS analysis on similar samples. They found that the Fe/Cr atomic ratio remained constant for the samples oxidized at 600 °C, whereas it increased dramatically for the support oxidized at 800 °C, symptomatic of the presence of a Fe-rich oxide on the outermost layer. For this high oxidation temperature, the thick oxide layer consisted of a Fe-rich layer sitting on top of a mixed Cr and Fe oxide phase.

Optical microscopy was employed to analyze the topological differences between un-oxidized and oxidized PSS supports. The surface of the original support was quite irregular, with several valleys and hills (not shown). The surface becomes smoother when the substrate is heated at 800 °C in flowing air (oxidized support).

The second investigated barrier was a washcoated thin layer of γ-Al_2O_3. Fig. 2c shows the diffraction pattern of the PSS substrate after washcoating with a suspension of γ-Al_2O_3 (15 wt.%), followed by calcination in air at 500 °C for 6 h. The XRD pattern only shows the peaks due to the γ-Fe phase observed in the unoxidized substrate. No γ-Al_2O_3 reflections were detected, probably due to the thinness of the deposited layer. Besides, at this low-calcination temperature, a small proportion of Fe, Ni and Cr oxides was observed. The thermal treatment led to a more intense γ-Fe peak suggesting an increase in the crystallinity of this phase.

To investigate the influence of the diffusion barriers on the porous size of the substrate, permeation measurements were performed. The nitrogen permeabilities (F_{N_2}) are summarized in Table 2. The modified supports show a significant decrease in the permeability values compared to the original PSS. Peña et al. [15] reported a He permeability of 58.2 $cm^3\,cm^{-2}\,min^{-1}\,bar^{-1}$ for the PSS substrate, and 11.3 $cm^3\,cm^{-2}\,min^{-1}\,bar^{-1}$ for the sintered support employing a similar oxidation treatment. Nam and Lee [5] in a stainless steel disk treated with Ni powder and silica sol, found nitrogen permeances as high as 450 $cm^3\,cm^{-2}\,min^{-1}\,bar^{-1}$, but their untreated substrate had an average pore size of 0.5 μm. The permeance of their substrate decreased around two orders of magnitude with the treatment.

3.1.2. Activated diffusion barrier

The seeding of metal nuclei is important for the deposition of a uniform film. The conventional seeding involves immersions in acid tin and palladium solutions. This process can introduce some impurities of tin onto the surface of the substrate. Kaliaguine and co-workers [16] suggested that tetravalent Pd(IV) oxides can coexist with tin on the activated substrates. Note that Pd(IV) is inactive towards hydrazine oxidation.

In view of this observation, a new activation method was assayed in this work. The palladium seeding was produced simultaneously with the washcoating of the PSS substrate with a γ-Al_2O_3 suspension and no tin salts were used. The PSS now covered with the Pd supported on the γ-Al_2O_3 was calcined in air and reduced in flowing hydrogen leading to the formation of the activated diffusion barrier.

Optical microscopy was employed to compare this new barrier with the γ-Al_2O_3/PSS support activated through the conventional method. The surface of the γ-Al_2O_3/PSS after Pd activation had a reddish brown color (pictures not shown) characteristic of the procedure [17]. The support change of color confirms the activation process. The optical micrograph of the support with the activated diffusion barrier shows a more important change of color, probably due to a higher dispersion of the Pd nuclei on the γ-Al_2O_3 layer.

Table 2
Nitrogen permeabilities (F_{N_2}) for the original and conditioned PSS substrate

Substrate	F_{N_2} ($cm^3\,cm^{-2}\,min^{-1}\,bar^{-1}$)
Original PSS	198.9
Oxidized PSS[a]	87.4
γ-Al_2O_3/PSS	40.6

[a] With air at 800 °C for 12 h.

3.2. Effect of annealing time over the formation of the Pd–Ag alloy

After the introduction of the oxide layers, Pd and Ag were sequentially deposited by the electroless plating technique. Three different kinds of membranes were prepared: Pd–Ag/α-Fe_2O_3/PSS, Pd–Ag/γ-Al_2O_3/PSS and Pd–Ag/(Pd)γ-Al_2O_3/PSS.

It is known that the formation of the Pd–Ag alloy proceeds through the atomic interdiffusion of silver and palladium after a long-term annealing. The effect of annealing time over surface alloy formation was studied over the PdAg/α-Fe_2O_3/PSS membrane. This membrane was cut in three fragments; two of them were annealed at 650 °C for 72 and 120 h, respectively. This process was followed through XRD, SEM, EPMA and Auger spectroscopy.

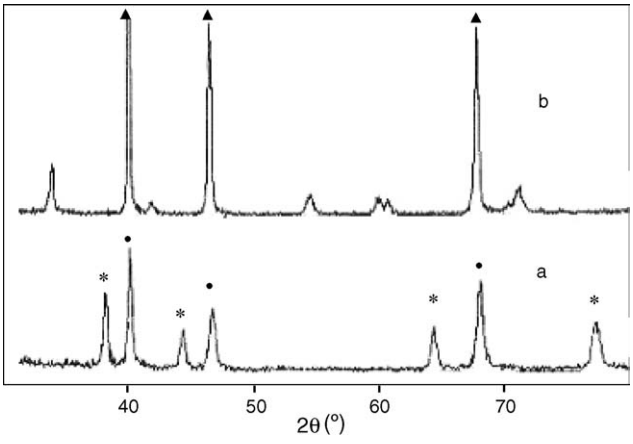

Fig. 3. XRD patterns of the Pd–Ag/α-Fe_2O_3/PSS membrane before (a) and after (b) annealing at 650 °C for 120 h. Symbols: (●) Pd, (*) Ag and (▲) Pd–Ag alloy.

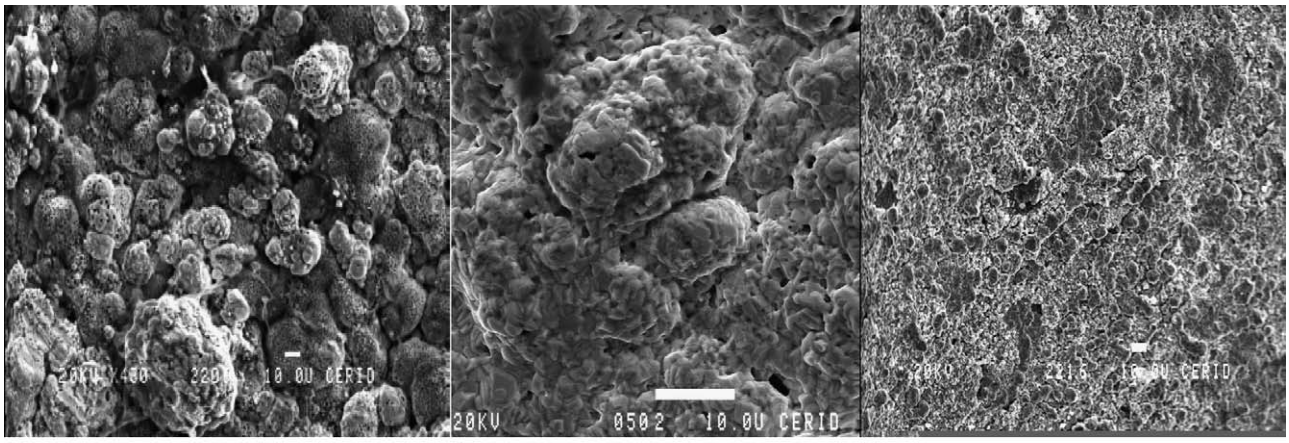

Fig. 4. Scanning electron micrographs of: (a) Pd–Ag/α-Fe_2O_3/PSS, (b)Pd–Ag/γ-Al_2O_3/PSS and (c) Pd–Ag/(Pd)γ-Al_2O_3/PSS.

Fig. 3 shows the X-ray diffraction patterns of the Pd–Ag composite membrane prepared on the oxidized support before and after annealing at 650 °C for 120 h. The 2θ angle values corresponding to the major reflection peaks for pure palladium [Pd (1 1 1)] and silver [Ag(1 1 1)] are $2\theta = 40.1^\circ$ and 38.1°, respectively (Fig. 3a). They are coincident with the peaks observed in the membrane previous to the thermal treatment. For the annealed Pd/Ag film, the reflection peaks (Fig. 3b) lie between those of pure metals, confirming that this layer is made up of a Pd–Ag alloy (fcc phase).

The alloy reflections exhibit a higher intensity and are better defined than those from Pd and Ag after deposition. The peaks assigned to Pd are more intense than the Ag reflections due to the greater proportion of palladium in the film. Because of this, the alloy peaks are displaced towards those of pure Pd. Besides, the reflections corresponding to α-Fe_2O_3 phase are observed.

Fig. 4a shows SEM pictures of the surface after electroless plating and annealing for 120 h. The surface morphology is uniform and smooth. In the micrograph, two phases can be distinguished, one darker than the other. Both phases present small pores. Höllein and coworkers [18] found a similar microstructure of the Pd film after permeation measurements at 500 °C.

Fig. 5 shows the Auger depth profiles of the film constituents with time of sputtering. The elements were monitored simultaneously. The rate of erosion was estimated in 1 Å/min. For the sample annealed during 72 h (Fig. 5a), the major component on the external surface was Pd; neither Ag nor Fe were present. This result indicates that no intermetallic diffusion of Ag and Fe occurred after the short treatment, and that no alloy was formed.

For the sample annealed for 120 h, the contents changed as follows (Fig. 5b): during the first minutes of sputtering only O and Fe were detected; after that the Pd and Ag content increased continuosly, keeping a Pd/Ag atomic ratio equal to 1. At approximately 500 min, the silver content remained constant with sputtering time, while the Pd signal kept increasing. The Pd/Ag ratio reached a value of 3 corresponding to 25% Ag at ca. 2000 Å. A long-term treatment of 120 h was needed to produce the Pd–Ag alloy formation at 650 °C. Fe and O were detected in all the depth analysed. The Fe/O ratio was constant suggesting the presence of Fe oxide in the Pd–Ag film and the interdiffusion of the PSS components.

Kaliaguine and coworkers [19] annealed the system under hydrogen flow to prevent membrane oxidation. However, the interaction between hydrogen and Pd favours the segregation of Pd from the Ag/Pd layer toward the membrane surface [12]. They

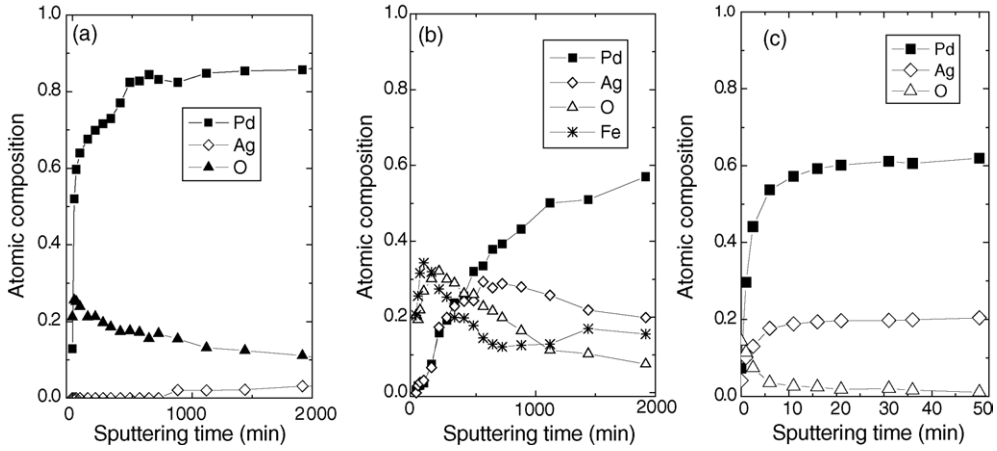

Fig. 5. Auger depth profiles for Pd–Ag/α-Fe_2O_3/PSS: (a) 72 h, (b) 120 h and Pd–Ag/γ-Al_2O_3/PSS (c)120 h.

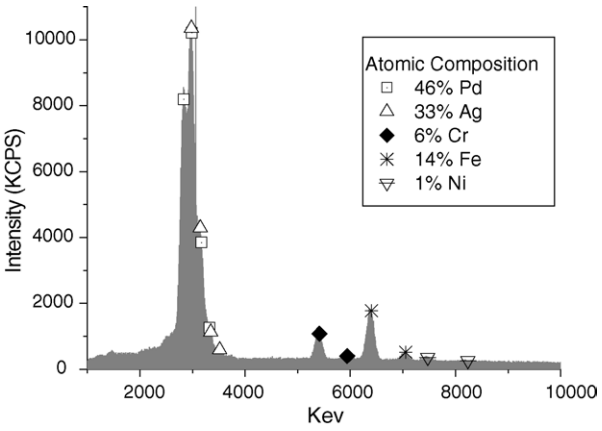

Fig. 6. EDS curve for Pd–Ag/α-Fe_2O_3/PSS annealed at 650 °C during 120 h.

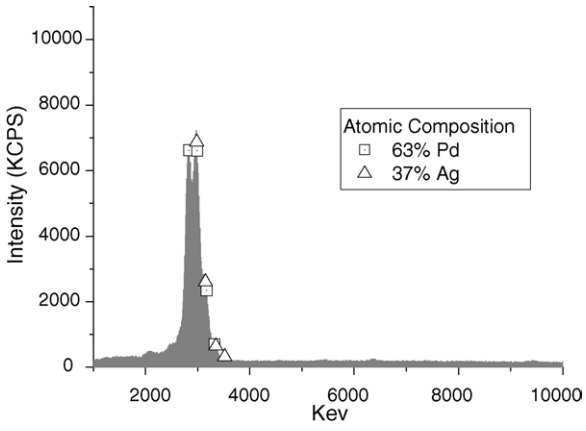

Fig. 7. EDS curve for Pd–Ag/γ-Al_2O_3/PSS annealed at 650 °C during 120 h.

employed an ultrathin intermediate layer of titanium nitride between Pd–Ag and the SS substrate. The Auger depth profiling indicated that those membranes were stable at temperatures as high as 700 °C.

The EPMA results of the Pd–Ag/α-Fe_2O_3/PSS external surface are shown in Fig. 6. The atomic composition was 46% Pd, 33% Ag, 14% Fe, 6% Cr and 1% Ni. These results are in agreement with the XRD patterns (Fig. 3b) and the Auger depth profiles (Fig. 5) supporting the intermetallic diffusion of the PSS constituents into the Pd–Ag layer.

3.3. Effect of the oxide layers on the intermetallic diffusion of stainless steel components through the Pd–Ag alloy

Fig. 5 compares the thermal behavior of the membranes with intermediate oxide layers: Pd–Ag/γ-Al_2O_3/PSS and Pd–Ag/α-Fe_2O_3/PSS. Both membranes were annealed at 650 °C for 120 h. The Auger depth profiling of the Pd–Ag/γ-Al_2O_3/PSS shows a homogeneous composition of Pd and Ag after 10 min of sputtering (Fig. 5c). The Pd/Ag ratio was equal to 3, which corresponds to 25% of Ag atoms. This ratio near the surface was lower probably due to the difference in surface tension between the metals. No Fe was detected during the Auger depth profiling, indicating that the intermetallic diffusion was stopped with the deposition of the alumina barrier.

This result was confirmed through EPMA analysis performed on the external surface of the Pd–Ag/γ-Al_2O_3/PSS membrane (Fig. 7). The atomic composition was 63 and 37% of Pd and Ag, respectively. The SEM micrograph (Fig. 4b) of the Pd–Ag/γ-Al_2O_3/PSS membrane shows a smoother and more homogeneous surface than Pd–Ag/αFe_2O_3/PSS. Thus, the Auger and EPMA results from Pd/Ag membranes annealed at 650 °C showed the alumina layer to be an effective intermetallic barrier. Nam and Lee [5] also found that an intermediate layer of silica introduced as a diffusion barrier between the palladium–copper alloy layer and the SS substrate improved the Pd–Cu composite membrane permeabilities.

However, in the case of the α-Fe_2O_3 layer, the diffusion of Fe was observed. It is possible that the oxide layer was insufficient to avoid the intermetallic diffusion through the alloy film. Rothenberger et al. [20], in membranes with diffusion barriers obtained by oxidation of the SS substract, observed a flux decrease following testing at 450 °C. Even though their characterization results were inconclusive, the intermetallic diffusion was not ruled out.

3.4. Membrane performance

Preliminary testing for defects due to pinholes were carried out at room temperature before annealing using nitrogen at pressure differences up to 5 bar. Under these conditions, negligible values of permeance were obtained for nitrogen in all the membranes. This implied that the composite membranes were dense.

After the thermal treatment of the membranes the gas-tightness (ρ) was checked with N_2 at temperatures up to 773 K and transmembrane pressures of 5 bar. Factor ρ is a function of substrate properties (surface roughness and average pore size) and preparation method and conditions [21]. High ρ values are usually necessary to secure high separation factors for composite membranes. The gas-tightness was found to be higher than 10^5 for Pd–Ag/Fe_2O_3/PSS, higher than 10^3 for Pd–Ag/γ-Al_2O_3/PSS and Pd–Ag/(Pd)γ-Al_2O_3/PSS. According to Jun and Lee [22], a gas tightness of 2×10^3 unambiguously indicates that the gas permeation flux would come mainly from dissolved hydrogen in the palladium lattice.

After thermal treatment, the nitrogen permeation (not shown) increased with decreasing temperature and increasing differential pressures in all the composite membranes. This indicates that nitrogen permeation through the membranes is via a Knudsen diffusion mechanism.

3.4.1. H_2 permeance

Fig. 8a shows the dependence of the hydrogen flux with the trans-membrane presssure differences at various temperatures for the Pd–Ag/Fe_2O_3/PSS composite membrane. The hydrogen flux increased with increasing temperature and differential pressure, as previously reported in the literature for Pd alloy composite membranes supported in a porous stainless steel [5]. The same trend was observed for the Pd–Ag/γ-Al_2O_3/PSS and Pd–Ag/(Pd)γ-Al_2O_3/PSS membranes (Fig. 8b and c). This is consistent with the solution-diffusion mechanism of hydrogen

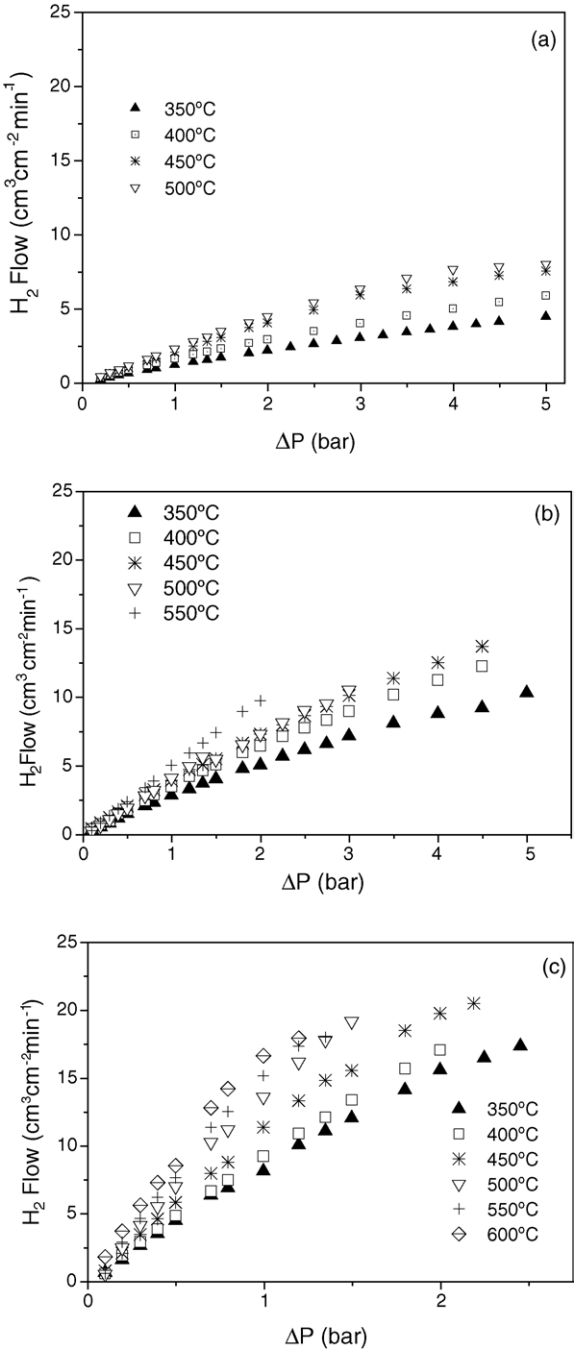

Fig. 8. Permeation measurements at different temperatures for: (a) Pd–Ag/α-Fe_2O_3/PSS, (b)Pd–Ag/γ-Al_2O_3/PSS and (c) Pd–Ag/(Pd)γ-Al_2O_3/PSS.

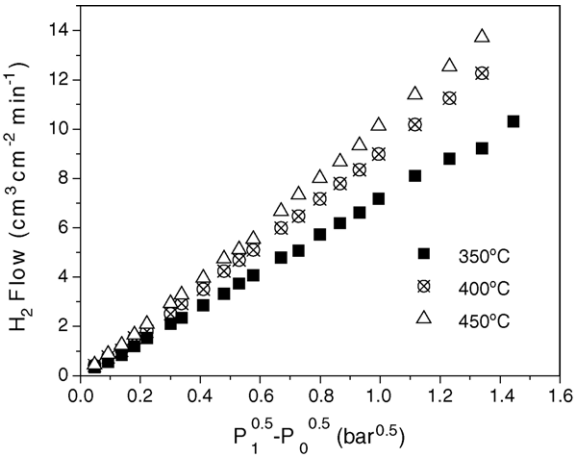

Fig. 9. Hydrogen flux at different temperatures for Pd–Ag/γ-Al_2O_3/PSS.

through palladium membranes [23]. Under this condition, the hydrogen flux should display a linear dependence on the difference of the square roots of inside and outside pressures. This is confirmed in Fig. 9 for the Pd–Ag/γ-Al_2O_3/PSS system. The same trend was observed for the other two membranes.

Permeance results for the prepared membranes at different temperatures are summarized in Table 3. Flux values were plotted against ($P^n_{H_2,ret} - P^n_{H_2,per}$), exponent n was allowed to float to a "best fit" value. The values of n are listed in Table 3. Xomeritakis and Lin [21] suggested that as thickness decreases, the H_2 permeation rate will reach a limiting value while the pressure exponent will be higher than 0.5. An exponent value of 0.5 is indicative of the hydrogen atoms forming an ideal solution in palladium, thus leading to a diffusion-limited transport mechanism, while a partial pressure exponent value approaching unity indicates that either a surface adsorption/dissociation or gaseous diffusion process is limiting [24]. Partial pressure exponent values in the range between 0.5 and 1.0 may be attributable to a mixed transport mechanism involving both surface effects entering and exiting the membrane as well as the hydrogen diffusion process occurring with comparable rates. Results quoted in the literature indicate that when very thin films are obtained, the value of the pressure dependence is unity [25]. However, for 20 μm or thicker, the pressure exponent does attain that for hydrogen atom diffusion of 0.5 [26]. The present values of n obtained with a Pd–Ag thickness of 16–20 μm are in agreement with the above conclusions for their intermediate thickness.

The hydrogen flux values obtained for the Pd–Ag/Fe_2O_3/PSS (Fig. 8a) are lower than those previously published. Yeung et al. [27] obtained a hydrogen flux value of 19 $cm^3\,cm^{-2}\,min^{-1}$ at 723 K using their Pd/stainless steel membrane. Dittmeyer et al. [28], on the other hand, measured a hydrogen flux of 12.5 $cm^3\,cm^{-2}\,min^{-1}$ at 673 K for a 5 μm thickness palladium film deposited on a stainless steel subtract with a pressure drop of 1 bar. However, our results for Pd–Ag/γ-Al_2O_3/PSS and Pd–Ag/(Pd)γ-Al_2O_3/PSS membranes at the same temperature and pressure drop provide values of 6.5 and 9.4 $cm^3\,cm^{-2}\,min^{-1}$, respectively. Allowing for the 16 μm thickness and the diffusion barrier of these membranes, they are in reasonable agreement with the previously quoted results. Values as high as 20.5 $cm^3\,cm^{-2}\,min^{-1}$ could be obtained in the Pd–Ag/(Pd)γ-Al_2O_3/PSS membrane at temperatures of 523 K and 2.2 bar of trans-membrane pressure.

In agreement with the literature [5,9], the lower hydrogen flux of Pd–Ag/Fe_2O_3/PSS could be attributed to metallic interdiffusion between the Pd–Ag film and the stainless steel support. The intermediate layer of γ-Al_2O_3 would explain the increased flux of H_2 in the Pd–Ag/γ-Al_2O_3/PSS. The Pd-alumina barrier improved the surface properties of the substrate leading to an even higher hydrogen flux in Pd–Ag/(Pd)γ-Al_2O_3/PSS.

Table 3
Hydrogen flux ($cm^3\ cm^{-2}\ min^{-1}\ bar^{-1}$) and n values of the composite membranes

Membrane		Temperature (°C)					
		350	400	450	500	550	600
Pd–Ag/α-Fe_2O_3/PSS	H_2 flow	2.69	3.86	5.40	6.70	–	–
	n[a]	0.55	0.52	0.52	0.46	–	–
Pd–Ag/γ-Al_2O_3/PSS	H_2 flow	6.81	7.09	7.95	6.50	4.84	–
	n[a]	0.51	0.59	0.59	0.59	0.69	–
Pd–Ag/(Pd)γ-Al_2O_3/PSS	H_2 flow	19.50	14.71	26.58	21.92	39.12	25.95
	n[a]	0.52	0.71	0.51	0.70	0.46	0.66

[a] Where n is the exponent in the Sievert's law expression, $J_{H_2} = F_{H_2}(P_1^n - P_0^n)$.

Another working parameter, load-to-surface ratio, was found to have significant effect on the value of hydrogen flux. L/S is defined as the ratio of flow rate of inlet gas mixture to the surface area of the Pd membrane tube. Increasing this value would raise the produced hydrogen flux [29]. The L/S ratio of our membranes varies between 1.1 and 1.2 $m^3\ h^{-1}\ m^2$. These are even lower than the lowest value reported by Lin and Rei [29]. They found for an $L/S = 2.1\ m^3\ h^{-1}\ m^{-2}$, a flux as low as 0.33 $cm^3\ cm^{-2}\ min^{-1}$. Thus, by increasing the L/S ratio the hydrogen flux of our membranes could be improved.

3.4.2. H_2 selectivity

Fig. 10 shows the hydrogen ideal selectivity, defined as the ratio of the permeance of hydrogen to that of nitrogen under the same trans-membrane pressure difference and temperature in the Pd–Ag/α-Fe_2O_3/PSS membrane. This ratio increased with temperature and decreased with trans-membrane pressure difference. This is consistent with nitrogen permeation by Knudsen diffusion and hydrogen by solution-diffusion in the

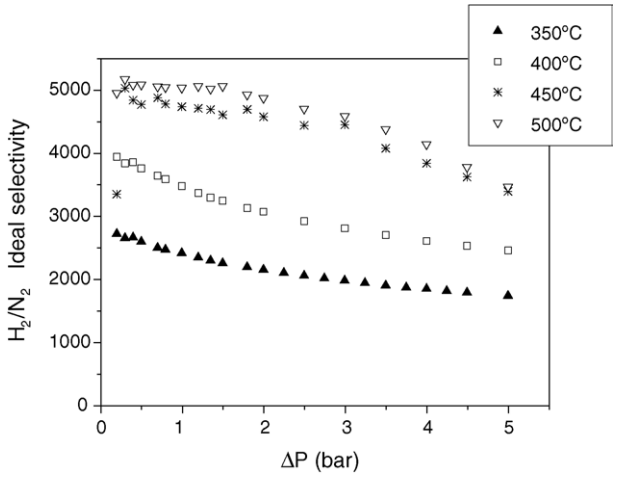

Fig. 10. Ideal hydrogen selectivities for the Pd–Ag/α-Fe_2O_3/PSS membrane.

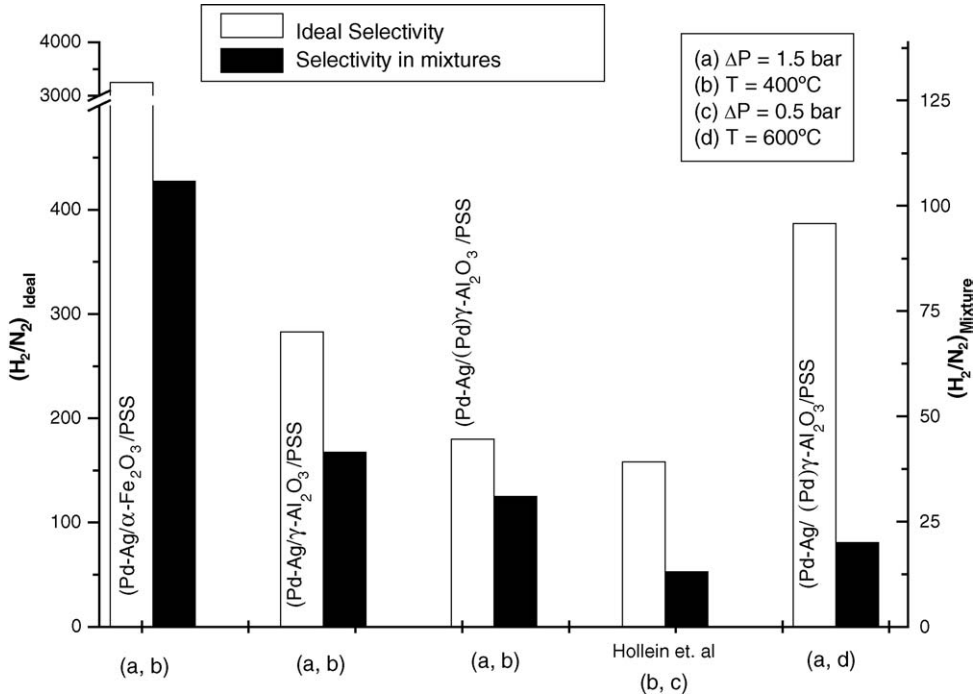

Fig. 11. Ideal and mixture hydrogen selectivities for Pd–Ag membranes.

palladium film [23]. On the other hand, Pd–Ag/γ-Al_2O_3/PSS and Pd–Ag/(Pd)γ-Al_2O_3/PSS showed lower ideal selectivity than Pd–Ag/α-Fe_2O_3/PSS but they are comparable to that reported by Höllein et al. [18] (Fig. 11). The present values of selectivities are in the range of 500–5000 for temperatures over 623 K, reported by Nam et al. [8] for the Pd alloy composite membranes coated onto stainless steel supports.

A comparison between the ideal selectivity values and those for binary H_2/N_2 mixture are presented in Fig. 11. A drastic drop in selectivity was observed, especially for Pd–Ag/α-Fe_2O_3/PSS, the selectivity decreased from 3248 to 106. A decrease in hydrogen flux when mixed gases were used was also observed by Li et al. [23]. Lee et al. [30] also found different permeation behavior for binary mixtures and simple gases. They concluded that, in the presence of hydrogen at high temperature, the oxide layers of the surface of the stainless steel substrate could be reduced. Accordingly, composite membranes with diffusion barrier (Pd–Ag/γ-Al_2O_3/PSS and Pd–Ag/(Pd)γ-Al_2O_3/PSS) suffer a less important decrease in the selectivity for binary mixture.

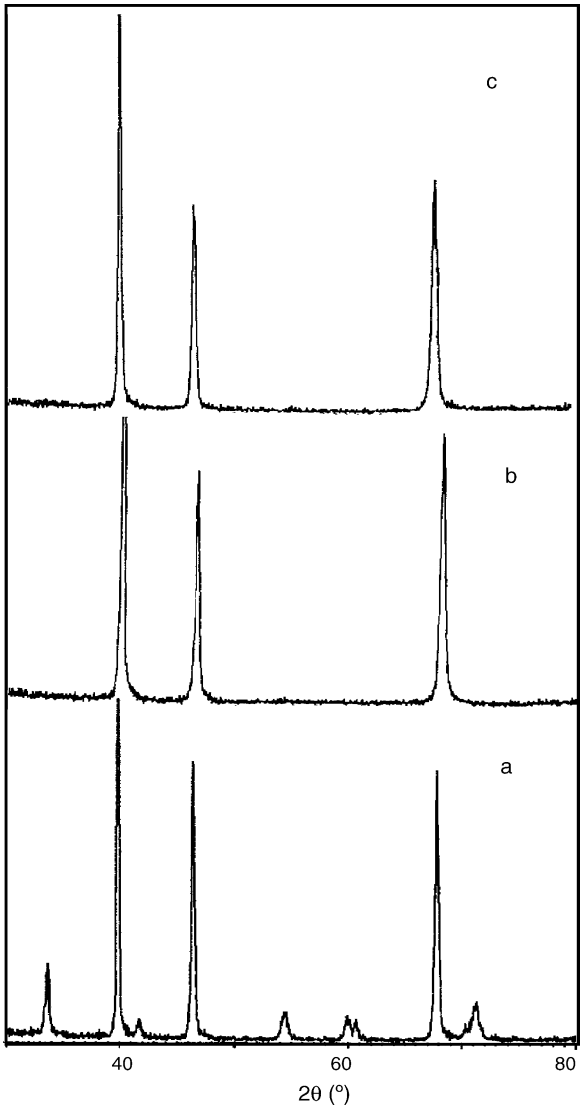

Fig. 12. XRD patterns of the Pd–Ag membranes after the permeation measurements. (a) Pd–Ag/α-Fe_2O_3/PSS, (b)Pd–Ag/γ-Al_2O_3/PSS and (c) Pd–Ag/(Pd)γ-Al_2O_3/PSS.

3.4.3. X-ray diffraction of the membranes after permeation measurements at high temperature

After the permeation measurements, the three membranes were characterized by X-ray diffraction to study the stability of the Pd–Ag layer. The diffraction pattern for the Pd–Ag/α-Fe_2O_3/PSS (Fig. 12a) exhibits the presence of α-Fe_2O_3 and the Pd–Ag alloy. However, the Pd–Ag/γ-Al_2O_3/PSS and Pd–Ag/(Pd)γ-Al_2O_3/PSS membranes only showed the reflections of the Pd–Ag alloy (Fig. 12b and c). These results, together with the values of permeance and selectivity, confirm the key role of an adequate diffusion barrier in composite membranes synthesized on PSS.

The intermetallic diffusion would explain the lower hydrogen flux and drastic mixture selectivity drop in Pd–Ag/α-Fe_2O_3/PSS. The intermediate layer of γ-Al_2O_3 effectively blocks this process, being responsible for the high values of permeance and the less important decrease in the selectivity for binary mixtures.

The composite membrane with activated diffusion barrier (Pd–Ag/(Pd)γ-Al_2O_3/PSS) presented high hydrogen flux (20.5 $cm^3\,cm^{-2}\,min^{-1}$), acceptable values of ideal selectivity and high stability at temperatures up to 600 °C.

4. Conclusions

The synthesized Pd–Ag/PSS membranes showed a good thermal stability. The membranes with alumina diffusion barriers exhibited an ideal selectivity lower than the Pd–Ag/α-Fe_2O_3/PSS one. However, the H_2 permeability of the former was two times higher. The Auger depth profile did not show the presence of Fe in the Pd–Ag film, indicating that the γ-Al_2O_3 layer effectively blocked the intermetallic diffusion. The composite membrane with activated diffusion barrier (Pd–Ag/(Pd)γ-Al_2O_3/PSS) appears as the most suitable one for high temperature hydrogen separation and for use in membrane reactors.

Acknowledgments

The authors wish to acknowledge the financial support received from UNL, CONICET and ANPCyT. They are also grateful to the Japan International Cooperation Agency. Thanks are given to Elsa Grimaldi for the English language editing and to the Surface Science Lab, INTEC, for the AES measurements.

References

[1] W. Lin, H. Chang, A study of ethanol dehydrogenation reaction in a palladium membrane reactor, Catal. Today 97 (2004) 181.
[2] J. Múnera, S. Irusta, L. Cornaglia, E. Lombardo, CO_2 reforming of methane as a source of hydrogen using a membrane reactor, Appl. Catal. A 245 (2003) 383.
[3] S. Tosti, A. Basile, G. Chiappetta, C. Rizzello, V. Violante, Pd–Ag membrane reactors for water gas shift reaction, Chem. Eng. J. 93 (2003) 23.

[4] A.K. Prabhu, A. Liu, L.G. Lovell, S.T. Oyama, Modeling of the methane reforming reaction in hydrogen selective membrane reactors, J. Membr. Sci. 177 (2000) 83.
[5] S. Nam, K. Lee, Hydrogen separation by Pd alloy composite membranes: Introduction of diffusion barrier, J. Membr. Sci. 192 (2001) 177.
[6] Y. Cheng, K. Yeung, Palladium–silver composite membranes by electroless plating technique, J. Membr. Sci. 158 (1999) 127.
[7] E. Gobina, K. Hou, R. Hugues, Equilibrium-shift in alkane dehydrogenation using a high-temperature catalytic membrane reactor, Catal. Today 25 (1995) 365.
[8] S. Nam, S. Lee, K. Lee, Preparation of a palladium alloy composite membrane supported in a porous stainless steel by vacuum electrodeposition, J. Membr. Sci. 153 (1999) 163.
[9] D. Wang, J. Tong, H. Xu, Y. Matsumura, Preparation of palladium membrane over porous stainless steel tube modified with zirconium oxide, Catal. Today 93–95 (2004) 689.
[10] Y.H. Ma, B. Ceylan Akis, M. Engin Ayturk, F. Guazzone, E.E. Engwall, I.P. Mardilovich, Characterization of Intermetallic diffusion barrier and alloy formation for Pd/Cu and Pd/Ag porous stainless steel composite membranes, Ind. Eng. Chem. Res. 43 (2004) 2936.
[11] S. Uemiya, T. Matsuda, E. Kikuchi, Hydrogen permeable palladium–silver alloy membrane supported on porous ceramics, J. Membr. Sci. 56 (1991) 315.
[12] J. Shu, B. Grandjean, E. Ghali, S. Kaliaguine, Simultaneous deposition of Pd and Ag on porous stainless steel by electroless plating, J. Membr. Sci. 77 (1993) 181.
[13] A. Li, G. Xiong, J. Gu, L. Zheng, Preparation of Pd/ceramic composite membrane 1. Improvement of the conventional preparation technique, J. Membr. Sci. 110 (1996) 257.
[14] S.G. Marchetti, R. Spretz, M.A. Ulla, E.A. Lombardo, Identification of the species formed in the Fe/MgO system: a Raman a Mössbauer study, Hyperfine Interact. 128 (2000) 453.
[15] M.A. Peña, D.M. Carr, K.L. Yeung, A. Varma, Ethylene epoxidation in a catalytic packed-bed membrane reactor, Chem. Eng. Sci. 53 (1998) 3821.
[16] J. Shu, B. Grandjean, E. Ghali, S. Kaliaguine, Autocatalytic effects in electroless deposition of palladium, J. Electrochem. Soc. 140 (11) (1993) 3175.
[17] P.P. Mardilovich, Y. She, Y.H. Ma, M.H. Rei, Defect-free palladium membranes on porous stainless-steel support, AIChE J. 44 (1998) 310.
[18] V. Höllein, M. Thornton, P. Quicker, R. Dittmeyer, Preparation and characterization of palladium composite membranes for hydrogen removal in hydrocarbon dehydrogenation membrane reactors, Catal. Today 67 (2001) 33.
[19] J. Shu, A. Adnot, B. Grandjean, S. Kaliaguine, Structurally stable composite Pd–Ag membranes: introduction of a diffusion barrier defect-free palladium membranes on porous stainless-steel support, Thin-Solid Films 286 (1996) 72.
[20] K. Rothenberger, A. Cugini, B. Howard, R. Killmeyer, M. Ciocco, B. Morreale, R. Enick, F. Bustamante, I. Mardilovich, Y. Ma, High pressure hydrogen permeance of porous stainless steel coated with a thin palladium film via electroless plating, J. Membr. Sci. 244 (2004) 55.
[21] G. Xomeritakis, Y. Lin, Fabrication of thin metallic membranes by MOCVD and sputtering, J. Membr. Sci. 133 (1997) 217.
[22] C. Jun, K. Lee, Palladium and palladium alloy composite membranes prepared by metal-organic chemical vapor deposition method (cold-wall), J. Membr. Sci. 176 (2000) 121.
[23] A. Li, W. Liang, R. Hughes, Characterisation and permeation of palladium/stainless steel composite membranes, J. Membr. Sci. 149 (1998) 259.
[24] B. Morreale, M. Ciocco, R. Enick, B. Morsi, B. Howard, A. Cugini, K. Rothenberg, The permeability of hydrogen in bulk palladium at elevated temperatures and pressure, J. Membr. Sci. 212 (2003) 87.
[25] S. Yan, H. Maeda, K. Kusabake, S. Morooka, Thin palladium membrane formed in support pores by metal-organic chemical vapor deposition method and application to hydrogen separation, Ind. Eng. Chem. Res. 33 (1994) 616.
[26] K. Hou, R. Hughes, Preparation of thin and highly stable Pd/Ag composite membranes and simulative analysis of transfer resistance for hydrogen separation, J. Membr. Sci. 214 (2003) 43.
[27] K. Yeung, R. Aravind, J. Szegner, A. Varma, Metal composite membranes: synthesis, characterization and reaction studies, Stud. Surf. Sci. Catal. 101 (1996) 1349.
[28] R. Dittmeyer, V. Höllein, K. Daub, Membrane reactors for hydrogenation and dehydrogenation processes based on supported palladium, J. Mol. Catal. A: Chem. 173 (2001) 135.
[29] Y. Lin, M. Rei, Separation of hydrogen from the gas mixture out of catalytic reformer by using supported palladium membrane, Sep. Purif. Technol. 25 (2001) 87.
[30] D. Lee, Y. Lee, S. Nam, S. Ihm, K. Lee, Study on the variation of morphology and separation behavior of the stainless steel supported membranes at high temperature, J. Membr. Sci. 220 (2003) 137.